Journal of Molecular Catalysis A: Chemical 328 (2010) 35–43

Contents lists available at ScienceDirect

Journal of Molecular Catalysis A: Chemical

journal homepage: www.elsevier.com/locate/molcata

Adsorption and reaction of CO and hydrogen on iron-based Fischer–Tropsch synthesis catalysts

Chenghua Zhang*, Guoyan Zhao, Kangkai Liu, Yong Yang, Hongwei Xiang, Yongwang Li

State Key Laboratory of Coal Conversion, Institute of Coal Chemistry, Chinese Academy of Sciences, Taoyuan South Road 27#, Taiyuan 030001, People's Republic of China

ARTICLE INFO

Article history:
Received 11 March 2010
Received in revised form 30 April 2010
Accepted 27 May 2010
Available online 4 June 2010

Keywords:
Fischer–Tropsch synthesis
Iron catalyst
H_2 adsorption
CO adsorption
Carbon hydrogenation

ABSTRACT

H_2, CO chemisorptions and the carbon hydrogenation on promoted iron Fischer–Tropsch synthesis (FTS) catalysts (Fe/SiO_2 and FeK/SiO_2) were investigated using temperature programmed surface reaction with X-ray photoelectron spectroscopy and laser Raman spectroscopy. It is found that potassium, used as promoter, does not lead to a distinct variation in the carbon species but changes the surface H/C ratio of carburized catalysts. Besides bulk iron carbide, several carbon species with different cluster sizes exist in the carburized catalysts, which have different reactivities towards hydrogen. The surface atomic carbon, the oligomerized carbon species and the bulk iron carbide are more reactive to hydrogen, whereas the large-size amorphous carbons are relatively inert to hydrogen. There is a good correlation between the chemisorption of H_2 or CO and the corresponding feed gas conversion activity in FTS reaction. Meanwhile, the methane selectivity is correlated with the hydrogenation capability of catalysts, indicating that the surface H concentration has an important effect on the selectivity of hydrocarbons.

1. Introduction

The depleting resource and increasing price of crude oil have revived the research interest for petroleum substitutes [1,2]. Based on Fischer–Tropsch synthesis (FTS) technology, carbon-containing resources (natural gas, coal and biomass) could be converted to clean liquid fuels and high-value chemicals. This process is considered as an alterative route to relax the pressure of depleting petroleum and would act as the foundation of the energy and chemical industry in post-oil era.

The FTS reaction is a typical CO hydrogenation on heterogeneous catalysts, which starts from the dissociation of CO and H_2 on transient metal surface and follows with the hydrogenation and polymerization of surface carbon species. Under reaction conditions, the working catalysts, especially for iron, are great reservoirs of carbons: bulk carbide, surface inactive carbon and surface active carbon. Using temperature-programmed techniques or transient methods, at least four kinds of carbon species have been indentified in iron catalysts [3–6]: (a) adsorbed, atomic carbon species; (b) amorphous, lightly polymerized carbon species; (c) iron carbides; and (d) graphitic surface carbon species. These carbon species play different roles in FTS reaction. For example, it is widely accepted that iron carbides are the active phases [7–11], which provide the active sites for CO activation and hydrogenation. At the same time, there is evidence [12,13] that the bulk carbide does not appreciably participate in the hydrocarbon synthesis. As for inactive carbons, some are inert while some are notorious poisons, such as graphite or coke. Different from the former two kinds of carbon species, surface active carbons are the key intermediates in CO hydrogenation, which have important influences on the activity, selectivity and stability of catalysts. Dwyer and Haredenergh [14] suggested that the competitive conversion of the reactive surface carbon to the surface polymeric carbon or graphitic carbon over the iron carbide surface determines the catalyst lifetime. Cao et al. [15] calculated the competitive reactions of surface carbon hydrogenation and coupling on $Fe_5C_2(0\,0\,1)$ surface from first principles. They found that the C–C coupling of the surface carbon is more favorable thermodynamically while the surface hydrogen will hinder C–C coupling and prevent the deactivation of $Fe_5C_2(0\,0\,1)$ surface.

In FTS reaction, methane is one of main products but not the objective products. Stockwell et al. [13] found that various hydrocarbons are likely to be originated from the same CH precursor. This indicates that the surface carbon hydrogenation to methane is competitive with the C–C coupling to the valuable high-molecular-weight hydrocarbons. Therefore, it is of great practical importance to investigate the hydrogenation of surface carbon species. In addition, potassium or alkali metals are the most effective promoters to suppress the formation of methane. At the moment, one question arises in one's mind. Which is the decisive factor for the methane formation, surface carbon species or alkali promoters?

In this study, the surface carbon species on carburized Fe/SiO_2 and FeK/SiO_2 catalysts were investigated using temperature-

* Corresponding author. Tel.: +86 351 7117176; fax: +86 351 7560668.
E-mail address: zhangchh@sxicc.ac.cn (C. Zhang).

1381-1169/$ – see front matter © 2010 Elsevier B.V. All rights reserved.
doi:10.1016/j.molcata.2010.05.020

programmed desorption and hydrogenation (TPD and TPH), Mössbauer effect spectroscopy, X-ray photoelectron spectroscopy (XPS) and laser Raman spectroscopy (LRS).

2. Experiments

2.1. Catalyst preparation

Two catalysts (Fe/SiO_2 and FeK/SiO_2) were used in this study. The Fe/SiO_2 precursor was prepared by continuous co-precipitation using $Fe(NO_3)\cdot 9H_2O$ (99.9%, Tianjin Chemical Co., PR China) and acidic silica sol (30 wt% SiO_2, Tianjin Chemical Co., PR China) as raw materials. The precipitation was carried out in a 4 L precipitated batch maintaining temperatures at 70 °C and pH value at 9.0 ± 0.1. The silica gel was added into ferric nitrate solution before precipitation with Fe/Si atomic ratio of 100/15. After precipitation, the precipitate was filtered. The filtered cake was consequently dried at 120 °C for 24 h and calcined at 500 °C for 5 h. The FeK/SiO_2 precursor was prepared through mechanically mixing certain amount of Fe/SiO_2 and $KHCO_3$. This kind of potassium addition method has been proved effective [16]. These catalysts have Fe/SiO_2 atomic ratio of 100/15 or Fe/K atomic ratio of 100/3.

2.2. Catalyst characterizations

A transient reaction system with on-line mass spectroscopy was used for TPD and TPH measurements. Gaseous feeds were controlled and metered using mass flow controllers. Gases were passed through a series of purification traps containing de-oxygen agent and zeolite to remove oxygen and water. The outlet of the microreactor was connected to a quadruple mass spectrometer (OmniStar 200, Balzers, Switzerland) through a capillary inlet system.

H_2 temperature-programmed desorption (H_2-TPD) was used to measure the hydrogen adsorption and desorption on H_2-reduced and CO-carburized catalysts. For H_2-TPD on H_2-reduced catalysts, the catalyst sample (100 mg) was firstly reduced in pure H_2 at 400 °C for 16 h and cooled to 50 °C. Then, the reduced sample was purged with Ar until the baseline of H_2 signal leveled off. Finally, the sample was heated to 800 °C at ramp of 10 °C/min. For H_2-TPD on carburized catalysts, the catalyst sample was firstly carburized in 5%CO/95%He at 300 °C for 5 h. Then, the feed gas was switched to He and the sample was flushed to 50 °C. At this temperature, the carburized sample was flushed with H_2 for 30 min and consequently purged with He until the baseline of H_2 signal leveled off. Finally, the sample was heated to 800 °C at ramp of 10 °C/min.

CO-TPD was used to measure the CO adsorption and desorption behavior on carburized catalysts. The catalyst sample (50 mg) was firstly carburized in 5%CO/95%He at 300 °C for 5 h and cooled to 50 °C. Then, the carburized sample was purged with He until the baseline of CO signal leveled off. Finally, the temperature was increased to 800 °C at ramp of 10 °C/min.

TPH was used to investigate the hydrogenation behavior of catalysts. Catalysts (50 mg) were loaded into the quartz tube reactor. The catalyst sample was firstly carburized in 5%CO/95%He at 300 °C for 5 h and cooled to 50 °C. Then, the carburized sample was flushed with pure H_2 until the signal leveled off. Finally, the temperature was increased to 800 °C at the heating rate of 10 °C/min.

In order to quantify the surface carbon species in catalysts, the catalyst samples were characterized with Raman spectrum and X-ray photoelectron spectroscopy (XPS) at different treatment stages in the TPH process. The objective of the work was to study the surface/bulk carbon species in carburized catalysts and their transformations in the TPH process. Therefore, three typical stages (after carburization, during the TPH and after the TPH) were chosen for the catalyst characterization. The carburization–hydrogenation treatments and the characterization protocols are presented in Fig. 1.

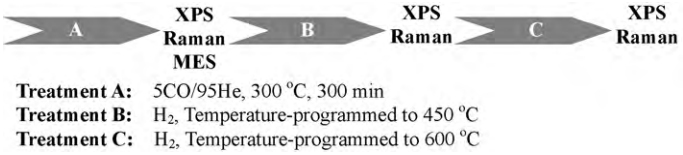

Fig. 1. Treatment and characterization protocols of Fe/SiO_2 and FeK/SiO_2 catalysts during carburization and hydrogenation.

The Mössbauer spectra of carburized catalysts were recorded at room temperature with a MR 351 constant-acceleration Mössbauer spectrometer (FAST, Germany), using a 25 mCi ^{57}Co (Pd) source. The spectrometer was operated in a symmetric constant acceleration mode. The spectra were collected over 512 channels in the mirror image format.

The XPS spectra were collected on a XPS analyzer (VG, Milti-Lab 2000), which has a monochromatized Mg Kα X-ray source (300 W). All binding energies of XPS spectra are calibrated with the peak position of adventitious carbon, which normally is adjusted to 284.6 eV. The relative surface concentrations of the metals were determined using the whole peak area of Fe 2p and C 1s and their corresponding sensitivity factors of 2.957 and 0.296, respectively. The Raman spectra were recorded on a Raman microscope instrument (Renishaw, UV–vis Raman 1000) equipped with an Argon ion laser ($\lambda = 514$ nm). The carbon content in the catalyst was analyzed using an automatic elemental analyzer (Elementar, Vario EL Cube, Germany).

2.3. Catalyst performance testing

The FTS experiments were conducted in a 12 mm i.d. stainless steel fixed-bed down-flow reactor with an effective bed length of approximately 15 cm (15 cm^3 bed volume). Approximately 3 g of catalyst was loaded in the isothermal region of the reactor. The remaining volume of reactor was filled with quartz granules with particle size of 10–20 and 20–40 mesh. All the catalysts were reduced in syngas with H_2/CO ratio of 2.0 (v/v) at 280 °C, 0.5 MPa, and 1000 h^{-1} for 16 h. The reaction conditions were controlled at 250 °C, 1.5 MPa, 4000 h^{-1} and $H_2/CO = 2.0$ (v/v).

3. Results and discussion

3.1. H_2 and CO chemisorptions

The catalysts were carburized in 5%CO/95%He at 300 °C for 300 min. Then the iron phase compositions of carburized catalysts were measured using Mössbauer spectroscopy, as listed in Table 1. It can be seen that catalysts after carburization contain iron carbide (Fe_5C_2) and superparamagnetic Fe^{3+} and Fe^{2+} oxides. Specifically, the Fe/SiO_2 catalyst contains 21.4% of iron carbide and 78.6% of iron oxides while the FeK/SiO_2 catalyst contains 56.5% of iron carbide and the remainder iron oxides.

In Fig. 2, the H_2-TPD curves of H_2-reduced catalysts are shown. It can be seen that the TPD curve of Fe/SiO_2 catalyst show an intense peak at about 100 °C and a group of overlapping peaks at above 300 °C. In the presence of potassium, all the peaks decrease markedly in intensity. As reported in literature [17], the H_2 thermal desorption peaks on Fe single crystal surfaces occurred at around 100 °C. In the present study, H_2 desorption peaks at about 100 °C are corresponding to the H species adsorbed on the metallic iron surface. The peaks at higher temperature may be due to the cleavage of OH species on the difficultly reduced oxide surface in catalysts.

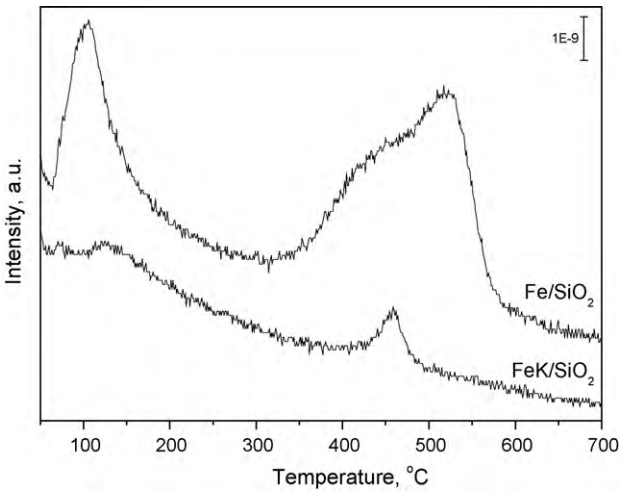

Fig. 2. H_2-TPD profiles on Fe/SiO_2 and FeK/SiO_2 catalysts reduced in pure H_2 at 400 °C for 16 h.

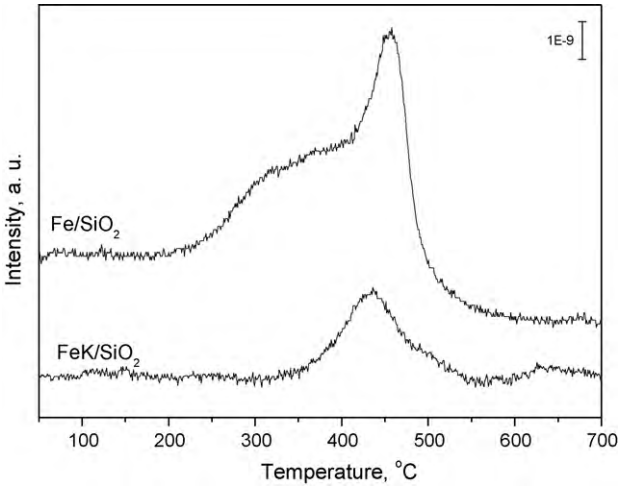

Fig. 3. H_2-TPD profiles on Fe/SiO_2 and FeK/SiO_2 catalysts carburized in 5%CO/95%He at 300 °C for 5 h.

In Fig. 3, H_2-TPD curves of CO-carburized catalysts are presented. As shown in Fig. 3, the H_2 adsorption on carburized catalysts produces H_2 desorption peaks at range of 250–500 °C. For Fe/SiO_2 catalyst, the H_2-TPD curve demonstrates a sharp peak at 455 °C and a somewhat less defined shoulder at lower temperature. In contrast, FeK/SiO_2 catalyst shows a peak at 435 °C and a broad shoulder at higher temperature. Moreover, the peak intensity of FeK/SiO_2 decreases sharply relative to that of Fe/SiO_2 catalyst. From the H_2-TPD curves, it is clear that there are two kinds of H adsorption sites, a weak H adsorption site at lower temperature and a strong H adsorption site at higher temperature, on carburized iron catalyst surface. Meanwhile, potassium suppresses the H_2 adsorption on carburized iron catalysts. Although iron carbides are considered as the FTS active phases, there is nearly no experimental report on the H_2 adsorption on iron carbide surfaces. The reason for this situation seems to be the difficulty to prepare a clean and single iron carbide surface or phase. However, there are a few of papers dealing with the chemisorption of hydrogen on iron surfaces [17,18–23]. On Fe(1 1 0), (1 1 0) and (1 1 1) single crystal surfaces, the hydrogen adsorption is dissociative and the initial adsorption energies are between 80 and 110 kJ/mol [17,21]. The corresponding H_2 thermal desorption peaks occurred at below 250 °C with heating rates in range of 5–20 °C/s [17,18,20,21]. Additionally, the H_2 desorption peaks on the carbon contaminated Fe(1 0 0) surface occurred at even lower temperatures [21,24]. In the present study, the H_2 desorption peaks on carburized catalysts occurred at above 250 °C, which are higher than those on iron crystal surfaces. These H_2 desorption peaks are not likely to result from the H species on Fe sites in carburized catalysts. Brucker and Rhodin [25] had suggested that the adsorption of hydrogen on a "carbonated" Fe(1 0 0) surface at −175 °C led to the formation of CH species. The theoretical calculation has indicated that, for H_2 adsorption on Fe_5C_2(0 0 1), (1 1 0) and (1 0 0) surfaces, the most stable surface species is CH. Meanwhile, the activation energies of CH_{ads} decomposition on transition metals are generally higher than 100 kJ/mol [15,26–28]. In this study, the MES results indicated that catalysts were not completely carburized and there were a large amount of iron oxides remained in catalysts. Therefore, H_2 desorption peaks on carburized catalysts appear to be a combination of the decomposition of surface CH species and the cleavage of surface OH species. From the H_2-TPD results, a direct evidence is that potassium apparently suppresses the H_2 adsorption on either H_2-reduced or carburized catalyst surfaces. It is in good agreement with reports that potassium is a very strong poison for H_2 dissociation [29,30].

In Fig. 4, CO–TPD curves of CO-carburized catalysts are presented. As shown in Fig. 4, the CO desorption peaks of catalysts all locate in temperature range of 300–600 °C. For Fe/SiO_2 catalyst, the CO desorption curve demonstrates a broad peak at 375 °C and a more intense peak at 468 °C. With the addition of potassium, the CO desorption peak intensity increases obviously and the peak position shifts to higher temperatures. Specifically, the FeK/SiO_2 catalyst shows a multi-peak overlapped curve with the maximum peak position at 548 °C and somewhat less defined shoulders at lower temperature. There are lots of papers studying on the CO adsorption on iron surfaces [19,21,31,32] but little work on iron carbide surfaces [33]. As reported in these studies, the CO adsorption on a clean Fe(1 0 0) surface resulted in four desorption peaks, which were designated as three molecular states at −23, 67, and 157 °C and a dissociative state at 527 °C [21,31,32]. The CO adsorption on a H_2-reduced iron catalyst [19] produced a similar CO desorp-

Table 1
MES parameters and iron phase composition of Fe/SiO_2 and FeK/SiO_2 catalysts carburized in 5%CO/95%He at 300 °C for 5 h.

Catalysts	Phase	Mössbauer parameters			
		IS, mm/s	QS, mm/s	Hhf, kOe	Area, %
Fe/SiO_2	χ-Fe_5C_2	0.40	−0.26	185	4.2
		0.22	0.22	218	11.0
		0.19	−0.16	105	6.2
	Fe^{3+} (spm)	0.30	0.94		69.3
	Fe^{2+} (spm)	1.02	1.66		9.3
FeK/SiO_2	χ-Fe_5C_2	0.29	−0.15	185	21.5
		0.25	0.10	219	11.3
		0.12	−0.04	108	23.7
	Fe^{3+} (spm)	0.35	0.92		42.7
	Fe^{2+} (spm)	0.87	1.54		0.9

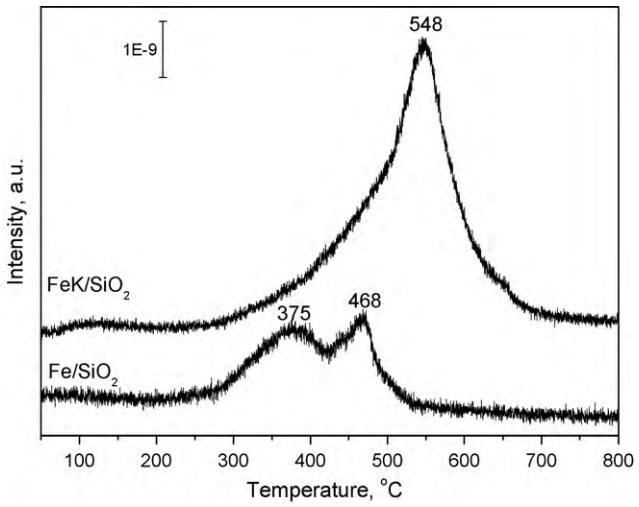

Fig. 4. CO–TPD profiles on Fe/SiO_2 and FeK/SiO_2 catalysts carburized in 5%CO/95%He at 300 °C for 5 h.

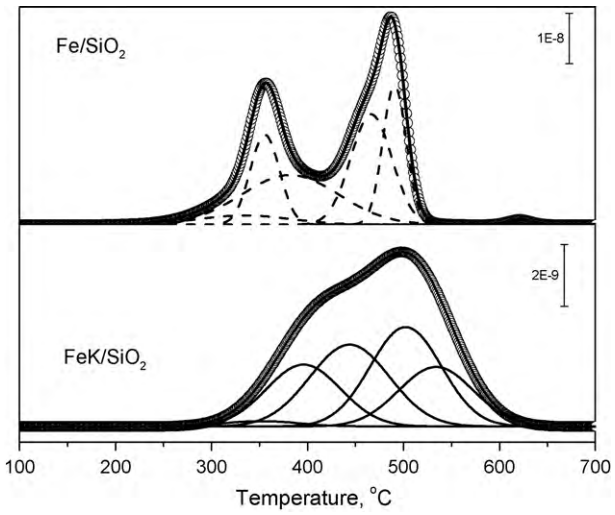

Fig. 5. TPH profiles of Fe/SiO_2 and FeK/SiO_2 catalysts carburized in 5%CO/95%He at 300 °C for 5 h.

tion shape as that on the Fe(1 0 0) surface. In our previous study [33], the CO–TPD curves on carburized iron catalysts were different from those on iron single crystal facets. In the present study, the CO adsorption on the carburized iron catalyst produced a totally different shape from that on the metallic iron surface. There are groups of overlapping peaks with maximum peak position at temperature range of 370–550 °C. The desorption temperatures of CO on carburized catalysts are far higher than those of the molecular CO on the Fe(1 0 0) surface and close to that of the dissociative CO. Benziger and Madix [21] estimated the activation energy for the dissociative CO desorption as 220 ± 20 kJ/mol (about 2.28 eV) on the Fe(1 0 0) surface. The first principle calculation of the CO adsorption on Fe_5C_2 surfaces [34] found that the adsorption energies of CO at multiple-iron-atom sites are generally below −2.10 eV. If desorbed in thermal flashing, the required temperature for the CO on Fe_5C_2 surfaces should be at about 500 °C, which is very close to the CO desorption temperatures in this study. Therefore, the CO–TPD peaks on carburized catalysts in the present study are likely to result from the strongly bound CO on Fe_5C_2 surfaces. A certain fact is that potassium largely improves the CO adsorption on carburized catalysts, which is consistent with the effect of potassium on the CO adsorption on iron surfaces [21,32,35].

3.2. TPH of surface carbon

Temperature-programmed surface reaction with hydrogen was used to study the hydrogenation behavior of surface carbon species on carburized catalysts. In this process, the main product of the carbon hydrogenation is CH_4. The curves of CH_4 evolution are shown in Fig. 5. It can be seen from the figure that CH_4 evolution peaks of the Fe/SiO_2 catalyst lie in the temperature range of 300–540 °C. These peaks are sharp and present a quite broad bottom, indicating that several overlapping peaks coexist. The CH_4 desorption curve of the FeK/SiO_2 catalyst presents a group of overlapping broad peaks in the temperature range of 300–600 °C. It is evident that the CH_4 peaks of FeK/SiO_2 catalyst shift to higher temperature compared with those of the Fe/SiO_2 catalysts. To quantitatively analyze the overlapping peaks, these TPH spectra were fitted with Gaussian curves to yield up several peaks and the corresponding peak parameters (temperatures and percent compositions) are listed in Table 2. From the table, it can be seen that four kinds of carbon species formed on catalyst surface according to the peak temperatures. It was reported that the reaction temperatures of adsorbed CO, atomic C and surface carbide with H_2 are in range of 270–390 °C [5]. Thus, the CH_4 desorbed peak in range of 340–360 °C can be ascribed to the hydrogenation desorption of atomic carbon on surface, which is signed as α carbon (C_α). The reaction temperature of carbon species with H_2 at 390–480 °C is similar with that of the oligomerized carbon species, which is signed as β carbon (C_β). There is one main carbon species reacted with H_2 at 490–550 °C, which is very close to the temperature of hydrogenation reaction of bulk carbides. Thus, this kind of carbon species is signed as γ carbon. The last carbon species on the catalysts surface is hydrogenated at above 600 °C close to the temperature of hydrogenation reaction of graphite. Thus, this kind of carbon species could be attributed to the graphitic carbon.

As shown in Table 2, the Fe/SiO_2 catalyst has relatively higher content of α carbon than the FeK/SiO_2 catalyst. Meanwhile, in the presence of potassium, the peak positions of different carbon species all shift to higher temperatures. It should be mentioned that there is a small amount of graphitic carbon on the Fe/SiO_2 catalyst rather than on the FeK/SiO_2 catalyst. One possible reason is that the Fe/SiO_2 catalyst produces graphite-like carbon species during the carburization while the FeK/SiO_2 does not. Another probable reason is that graphitic carbon forms on both catalysts, whereas the hydrogenation capability of the Fe/SiO_2 catalyst is strong enough to hydrogenate the graphitic carbon to methane. Actually, the MES results have proved a relatively lower carburization degree of the Fe/SiO_2 catalyst. At the same time, Table 2 also lists the carbon contents and the total peak areas of CH_4 evolution on both carburized Fe/SiO_2 and FeK/SiO_2 catalysts. As shown in the table, the carbon content in the carburized Fe/SiO_2 catalyst is one fourth of that in the carburized FeK/SiO_2 catalyst while the total amount of carbon hydrogenation to CH_4 during TPH process on the Fe/SiO_2 catalyst is fourfold higher than that of the FeK/SiO_2 catalyst. According to MES and TPH results, the FeK/SiO_2 catalyst has higher carbide content after the carburization but produces lower CH_4 amount in TPH, indicating that a large amount of carbon species in the FeK/SiO_2 catalyst could not be hydrogenated to CH_4 during the TPH process. It also indicates that potassium suppresses the carbon hydrogenation, which is consistent with the H_2-TPD results.

3.3. Surface carbon species

Although TPH provides the information of most carbon species on the catalyst surface, a large amount of carbon species are not shown in TPH spectra. So, XPS and Raman methods were used to

Table 2
The carbon content of carburized catalysts, peak parameters of individual carbon species and CH_4 total areas in TPH process for Fe/SiO_2 and FeK/SiO_2 catalysts carburized in 5%CO/95%He at 300 °C for 5 h.

Catalysts	C[a], wt.%	Peak parameters[b,c]						CH_4 total area[d]
		C_α	C_β		C_γ		C_δ	
Fe/SiO_2	1.19 ± 0.07	5.2/335	16.3/356	29.7/382	27.9/466	20.2/491	0.7/621	418.8
FeK/SiO_2	4.34 ± 0.02	1.8/352	19.9/396	28.3/444	30.7/502	19.3/534		104.5

[a] The carbon content was measured by element analysis.
[b] The TPH profiles were fitted by multiple Gaussian shapes.
[c] The percentage composition (%)/the peak position (°C) of individual carbon species.
[d] The total area (a.u./g_{-Fe}) is obtained by integrating the whole CH_4 evolution curves.

identify the detailed structure of these carbon species on carburized catalysts.

In Fig. 6, the K 2p and C 1s XPS spectra of catalysts are shown. Each XPS spectrum was fitted by means of an iterative nonlinear least-squares procedure with Gaussian bands. As shown in the figure, all C 1s spectra show a group of overlapping peaks with binding energies (E_B) from 280 to 289 eV. The energy difference of C 1s core level is associated with its change from an oxidized state ($C^{\delta+}$) in the O–C–metal bond to a reduced state ($C^{\delta-}$) in the C-metal bond [32]. Using Gaussian fitting, the C 1s spectrum could be divided into several peaks, which are attributed to oxide species, elemental carbon, and reduced species, respectively. As identified in literature for carbonaceous species on iron surface, the bands with E_B in range of 286.0–289.0 eV are attributed to carbonates [36], in range of 285.0–286.0 eV to carbonyl species [36–38], and at 284.6 eV to graphitic carbon. The low binding energy components (<284.0 eV) are attributed to the carbonaceous species in a reduced state whereas the more detailed chemical structure of these species is difficult to be obtained from the XPS measurement. Through controlling carbon deposition parameters (CO/H_2 ratio, temperature and time), Krebs et al. [39,40] obtained, on iron crystals, three significantly different surface carbon phases (named as phases I, II and III) depending on the amount of the bonded hydrogen. With the aid of AES and XPS, the phase I was designated to atomic carbon, CH, CH_2, CH_3 as well as polymerized C_nH_m groups with E_B (C 1s) = 283.9 eV, which contain a large amount of hydrogen. The phase II contains less bonded hydrogen than phase I and was characterized as a carbidic carbon layer with E_B (C 1s) = 284.2 eV. The phase III was attributed to graphitic carbon with E_B (C 1s) = 284.7–285.0 eV depending on the amount of intercalated hydrogen. In the present study, the low binding energy components with E_B at 283.5–284.0 eV and below 283.0 eV could be attributed to carbidic carbon–hydrogen and Fe–CH_x, respectively, considering these species being abundant after hydrogenation. The corresponding fitting parameters of C 1s XPS spectra of catalysts with different treatment protocols are given in Table 3. As shown in the table, the most abundant surface species is graphitic carbon on catalysts with treatment A. With treatment B, there is little effect on surface carbonates and carbonyls. However, the relative intensity of graphitic carbon band decreases and the band position shifts to lower binding energy. With treatment C, the relative intensities of carbonates, carbonyls and graphitic carbon decrease apparently and the most abundant species shifts to hydrogen-rich species (carbidic carbon or Fe–CH_x). Comparison of two catalysts, there is no essential difference in surface carbon species except that the Fe/SiO_2 catalyst has slightly higher content of Fe–CH_x species than the FeK/SiO_2 catalyst. Through integrating Fe 2p and C 1s spectra, the surface C/Fe mole ratios of catalysts are calculated and listed in Table 3. It can be seen that the C/Fe mole ratios of both catalysts increased with sequential treatments. It is reasonable for the increased C/Fe ratio after carburization because the carburization of catalysts is a process of carbon deposition on metal surface and subsequent surface carbon dissolving into bulk phase. With the treatments of the hydrogenation, the surface C/Fe ratios also increased greatly. The hydrogenation of the carburized catalysts is a reaction of surface carbon with hydrogen to methane and a concomitant diffusion of bulk carbon out to surface. The increased surface C/Fe ratios after hydrogenation indicate that a considerable carbon species are inert to hydrogen. They deposit on catalyst surfaces even under severe hydrogenation

Table 3
The surface C/Fe ratio[a] and C 1s XPS band parameters[b] of surface carbon species for Fe/SiO_2 and FeK/SiO_2 catalysts with different treatments during carburization and hydrogenation.

Catalysts	Treatment A	Treatment B	Treatment C
Fe/SiO_2			
C/Fe ratio	0.72	1.95	2.26
Fe–CHx			282.7/1.3/14
			281.3/1.8/23
Carbidic carbon	284.0/1.3/15	283.9/1.3/45	283.8/1.3/21
Graphitic carbon	284.6/1.2/37	284.6/1.2/26	284.6/1.2/19
Carbonyl	285.4/1.2/20	285.5/1.2/20	285.4/1.2/9
Carbonates	288.4/1.35/17	288.3/1.35/9	288.0/1.35/6
	286.6/1.4/11		286.6/1.4/9
FeK/SiO_2			
C/Fe ratio	0.84	0.99	353.22
Fe–CHx		282.5/1.3/6	282.8/1.3/12
			281.6/1.3/20
Carbidic carbon	283.7/1.3/23	283.9/1.3/18	283.7/1.3/25
Graphitic carbon	284.6/1.2/41	284.6/1.2/33	284.6/1.2/15
Carbonyl	285.4/1.2/19	285.4/1.2/13	285.7/1.2/8
Carbonates	288.8/1.35/7	288.3/1.35/17	288.3/1.35/7
	287.7/1.4/11	286.9/1.4/12	286.9/1.4/13

[a] The surface C/Fe ratio was determined from the C 1s and Fe 2p XPS spectra.
[b] The binding energy (eV)/bandwidth (eV)/percentage of each band area relative to the total C 1s spectrum area.

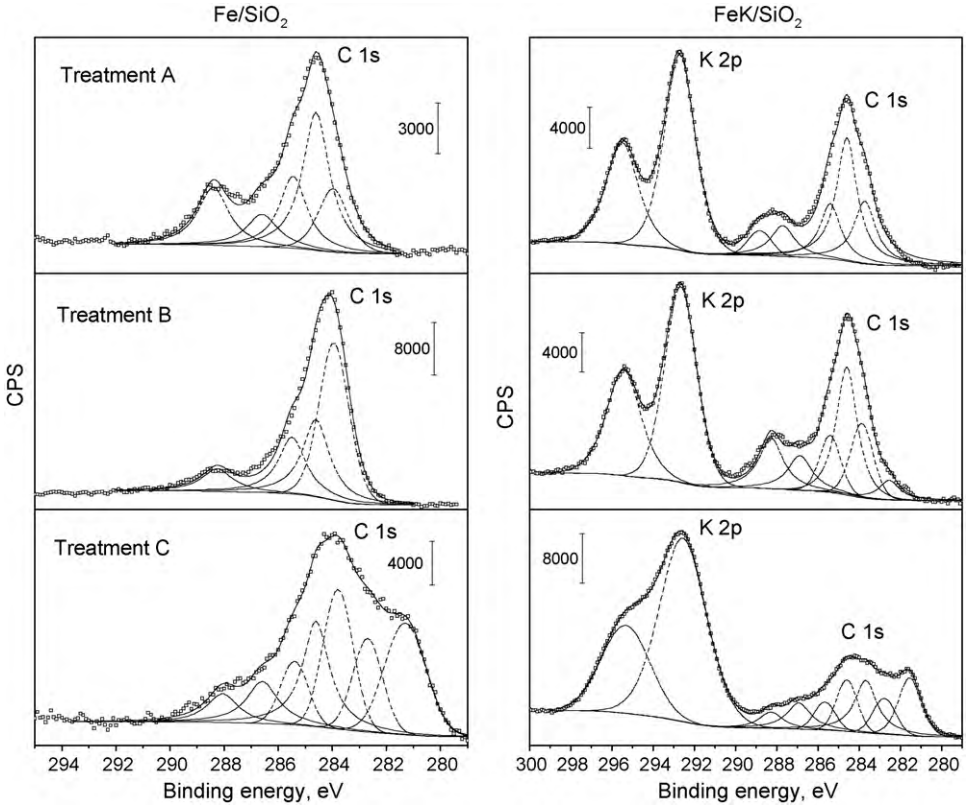

Fig. 6. C 1s and K 2p XPS spectra of Fe/SiO_2 and FeK/SiO_2 catalysts with different treatments during carburization and hydrogenation.

conditions. Comparison of two catalysts, especially for catalysts with treatment C, it is found that the surface C/Fe ratio of the FeK/SiO_2 catalyst is far higher than that of the Fe/SiO_2 catalyst. These results indicate that potassium has no essential effect on the surface carbon species but suppresses their reactivities towards hydrogen.

In Fig. 7, the Raman spectra of catalysts with different treatments are shown. It can be seen that Raman spectra of carburized catalysts show two broad bands at 1350 and 1600 cm^{-1} and a shoulder at 1450 cm^{-1}. The Raman spectra of the FeK/SiO_2 catalyst do not change with the variation of treatment protocols. However, the Raman spectrum of the Fe/SiO_2 catalyst totally changes after treatment C. The bands at 1350 and 1600 cm^{-1} become weaker while the band at 1450 cm^{-1} becomes stronger apparently accompanied several new bands at 1050, 1160 and 1300 cm^{-1}. As reported in literature [41,42], the band at around 1600 cm^{-1} could be attributed to the in-plane bond-stretching motion of pairs of C sp^2 atoms, usually occurring in graphite and named as G band. This mode does not require the presence of sixfold ring, and so it occurs at all sp^2 sites, not only those in rings. The band at 1350 cm^{-1} could be assigned to the breathing mode of A_{1g} symmetry (D band) of graphitic carbon. This mode is forbidden in perfect graphite and only becomes active in the presence of disorder. Its intensity is directly dependent on the presence of sixfold aromatic ring. The width of the D band is correlated to a distribution of sp^2 bonded clusters with different ring sizes [41,43]. The band at 1450 cm^{-1} could be assigned to the vibration of the hydrogens of the $-CH_2-$ group in hydrocarbons [44]. The band at 1300 cm^{-1} could be attributed to the vibration of a methyl group against the rest of the molecule and the bands at 1000–1200 cm^{-1} could be ascribed to the vibration of carbon atoms in straight chain hydrocarbons with more than seven carbon atoms [44]. From Raman analysis, the carbon species on carburized catalysts are mostly amorphous carbon and a small amount of hydrocarbons. After hydrogenation, there is a marked increase in the intensity of hydrocarbons on the Fe/SiO_2 catalyst while there is little change on the FeK/SiO_2 catalyst.

The Raman spectra could be fitted by asymmetric Breit–Wigner–Fano curves for the G peak and Lorentzian curves for D and other peaks [41]. For Raman spectra of amorphous carbon, the intensity ratio of D- and G-peaks (I_D/I_G) is proportional to the number and clustering of rings when the dimensions are under 20 Å. Ferrari and Robertson [41] proposed a relation between I_D/I_G and the in-plane correlation length or cluster diameter (La):

$$\frac{I_D}{I_G} = C(\lambda)\, L_a^2 \quad (1)$$

where I_D and I_G are heights or integrated intensities of the D-peak and G-peak, respectively. The parameter C is wavelength dependant and in this work C(514 nm) is about 0.0055. Using Eq. (1), the cluster diameter of surface amorphous carbon on catalysts was calculated and shown in Table 4. It can be seen from the table that the average cluster size of amorphous carbon is close to 11 Å for both carburized catalysts, and the size increases after hydrogenation treatments (B and C). This is possibly in that the smaller carbon cluster is easily removed with hydrogenation, whereas the larger carbon cluster remained on catalyst surfaces. Comparison of both catalysts, it can be also found that, after treatment C, the carbon cluster of the Fe/SiO_2 catalyst is larger than that of the FeK/SiO_2 catalyst. These results indicate that the Fe/SiO_2 catalyst has stronger hydrogenation capability while potassium inhibits the hydrogenation of surface carbon species.

3.4. FTS performance

The FTS activity and selectivity of catalysts are listed in Table 5. It can be seen that the Fe/SiO_2 catalyst shows CO conversion of 34.3% and H_2 conversion of 30.9%. On FeK/SiO_2 catalyst, the CO conversion is markedly increased to 58.3% while the H_2 conversion is decreased

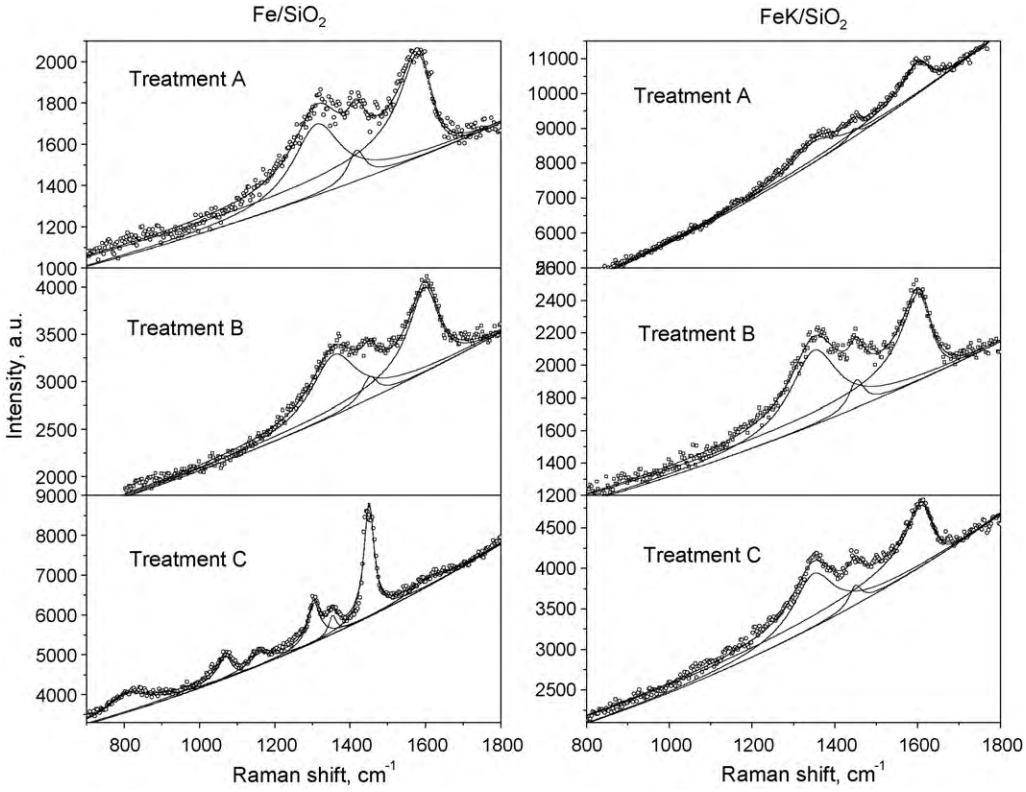

Fig. 7. Raman spectra of Fe/SiO_2 and FeK/SiO_2 catalysts with different treatments during carburization and hydrogenation.

Table 4
In-plane correlation length (L_a) of surface amorphous carbon by fitting Raman spectra of Fe/SiO_2 and FeK/SiO_2 catalysts with different treatments during carburization and hydrogenation.

Catalysts	Treatment A			Treatment B			Treatment C		
	G position, cm^{-1}	I_D/I_G	L_a, Å	G position, cm^{-1}	I_D/I_G	L_a, Å	G position, cm^{-1}	I_D/I_G	L_a, Å
Fe/SiO_2	1597.4	0.7	11.5	1597.7	0.7	11.5	1608.0	2.4	20.9
FeK/SiO_2	1598.8	0.7	11.3	1599.4	0.9	12.8	1607.0	1.0	13.2

to 25.4%. For the product selectivity, Fe/SiO_2 catalyst produces relatively higher CH_4 and lower C_5^+ hydrocarbons. It is evident that potassium suppresses the hydrogenation activity, lowers the CH_4 selectivity, and enhances the C_5^+ selectivity.

As indicated by characterization results, potassium apparently suppresses the H_2 adsorption, largely enhances the CO adsorption, and hence decreases the hydrogenation capability of catalysts. It was found that H_2 or CO conversion in FTS reaction correlates well with the corresponding gas chemisorption. Meanwhile, the CO conversion to long-chain hydrocarbons is improved and the CO hydrogenation to methane is suppressed by the promotion of potassium in FTS reactions. However, there is no obvious evidence to indicate a distinct carbon species on the potassium promoted catalyst. It is evident that the surface H/C ratio plays an important role in determining the hydrocarbon selectivity of the iron FTS catalyst. The role of potassium is likely to change the surface H/C ratio on the catalyst surface.

Based on above results and discussion, a scheme for the formation and transformation of carbon species on iron FTS catalysts could also be outlined as shown in Fig. 8.

The carbon species stem from the dissociation of chemisorbed CO, which involves two weakly bound molecular CO states (α_1 and α_2), a strongly bound π-CO state (α_3) and a dissociated CO state (β) on iron surface [31,32]. The adsorbed carbon atoms (C_{ads}) are very reactive and further transform at least in three pathways. Firstly, these surface atomic C_{ads} species can dissolve in the interstitial vacancies of iron phase and form iron carbides (Fe_xC) indepen-

Table 5
Activity and selectivity of Fe/SiO_2 and FeK/SiO_2 catalysts for FTS reaction in a fixed-bed reactor.

Catalysts[a]	Activity, %		CO_2[b], %	HC selectivity[c], wt.%			$C_{2-4}=/C_{2-4}$
	CO conversion	H_2 conversion		CH_4	C_{2-4}	C_5^+	
Fe/SiO_2	34.3	30.9	7.1	11.1	25.2	63.7	0.58
FeK/SiO_2	58.3	25.4	33.1	2.8	17.8	79.4	1.00

[a] Reaction condition: $H_2/CO = 2.0$ (v/v), 250 °C, 1.50 MPa, 4000 h^{-1}.
[b] CO_2 is the molar selectivity of CO conversion to CO_2.
[c] Hydrocarbon selectivities are reported on the basis of total hydrocarbon in weight.

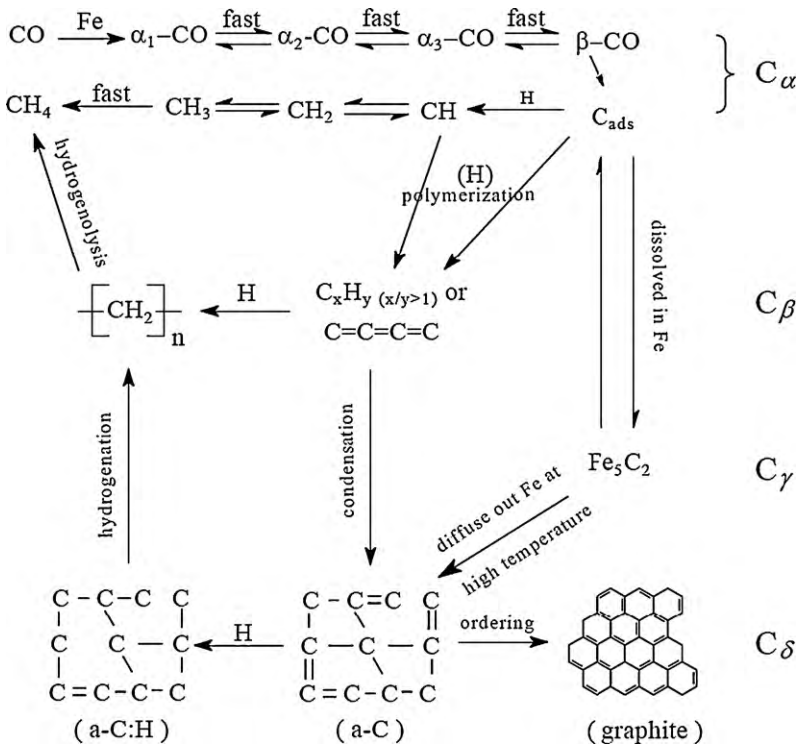

Fig. 8. The proposed conversion of surface and bulk carbon species on iron-based FTS catalysts in carburization and hydrogenation.

dent of hydrogen [45]. Secondly, in the presence of hydrogen the C_{ads} species can easily convert to surface methylidyne (CH) since CH is the most stable species on iron surfaces [46]. Thirdly, if in absence of hydrogen, the surface carbon species could also polymerize to large size carbon clusters because these carbon species are thermodynamically favorable [15]. The surface CH species can be subsequently hydrogenated to surface CH_2, CH_3 and gaseous CH_4. This pathway is the main channel of methane production in FTS reaction. The C–C coupling of C_α species to C_β species involves not only the atomic carbon but the CH species, i.e. C + C, CH + CH and C + CH reactions. This is plausible because the C and CH species [27,40,46] as building blocks rather than CH_2 or CH_3 species [47] was supported by experimental and theoretical studies on Fe, Co and Ru surfaces. Here, one would find that CH is a key crotch for the branching of product pathways to methane or to long-chain hydrocarbons. The modification of the reactivity of CH towards hydrogen may be a valid method to control the production of methane (for example, the addition of potassium in this study). The oligomer of carbon (C_β) is difficult to detect or distinguish from amorphous carbon (a-C) and graphite in the present experiment. The C_β species may be the common reactive intermediate for hydrocarbons and amorphous carbon depending on the surface concentration of hydrogen. Under the FTS atmosphere, the building blocks (C or CH) polymerize to C_β and further hydrogenates to hydrocarbons. In the lean hydrogen atmosphere, the C_β further condense to larger size amorphous carbon cluster and finally to graphite. Under more severe condition (higher temperatures) and with excess of hydrogen, the amorphous carbon could be hydrogenated to amorphous carbon–hydrogen (a–C:H) film and hydrocarbons while graphite is relatively inert. The bulk carbon in iron carbide can diffuse out from the bulk phase, hydrogenate to methane or directly form amorphous carbon. The C–C bond in hydrocarbon and amorphous carbon could cleave to methane by hydrogenolysis at different temperatures depending on their reactivities to hydrogen [48].

4. Conclusions

Two Fe/SiO_2 catalysts promoted with or without potassium were used to study the surface chemisorption and the surface carbon hydrogenation behavior.

On H_2-reduced catalysts, hydrogen mainly adsorbs on the surface iron sites and the surface oxide sites. On CO-carburized catalysts, hydrogen probably exists as the most stable CH or OH species. The CO adsorption on carburized catalysts may be the strongly bound CO on Fe_5C_2 surfaces.

According to the reactivity towards hydrogen, the carbon species on carburized catalysts could be categorized into four classes: (a) atomic carbon, (b) oligomerized carbon, (c) iron carbide, and (d) graphitic carbon. According to the binding energy of C 1s XPS spectra, the surface carbon species include carbonates, carbonyl, graphite, carbide, and Fe–CH_x. In LRS results, the surface carbon species are mainly amorphous carbons with different cluster sizes and long-chain hydrocarbons. The small-size amorphous carbons are more reactive to hydrogen while the large-size carbons are inert to hydrogen.

Potassium apparently suppresses the H_2 adsorption, largely improves the CO adsorption and decreases the hydrogenation activity of catalysts. The role of potassium is to decrease the surface H/C ratio while it dose not lead to any distinct carbon species on the catalyst surface. With the decrease of the surface H/C ratio, the H_2 conversion decreases, the CO conversion increases, and hydrocarbon products shift to long-chain molecules.

Acknowledgements

We thank the National Outstanding Young Scientists Foundation of China (20625620), and the National Natural Science Foundation of China (20703054). This work is also supported by Synfuels CHINA. Co., Ltd.

References

[1] Z. Liu, S. Shi, Y. Li, Chem. Eng. Sci. 65 (2010) 12–17.
[2] Y. Traa, Chem. Commun. 46 (2010) 2175–2187.
[3] J. Galuszka, T. Sano, J.A. Sawicki, J. Catal. 136 (1992) 96–109.
[4] S.A. Eliason, C.H. Bartholomew, Stud. Surf. Sci. Catal. 111 (1997) 517–526.
[5] J. Xu, C.H. Bartholomew, J. Phys. Chem. B 109 (2005) 2392–2403.
[6] D. Bianchi, L.M. Tau, S. Borcar, C.O. Bennett, J. Catal. 84 (1983) 358–374.
[7] J.F. Shultz, W.K. Hall, T.A. Dubs, R.B. Anderson, J. Am. Chem. Soc. 78 (1956) 282–285.
[8] R. Dictor, A.T. Bell, J. Catal. 97 (1986) 121–136.
[9] K.R.P.M. Rao, F.E. Huggins, V. Mahajan, G.P. Huffman, V.U.S. Rao, B.L. Bhatt, D.B. Bukur, R.J. O'Brien, Top. Catal. 2 (1995) 71–78.
[10] L.D. Mansker, Y. Jin, D.B. Burker, A.K. Datye, Appl. Catal. A 186 (1999) 277–296.
[11] S. Li, G.D. Meitzner, E. Iglesia, J. Phys. Chem. B 105 (2001) 5743–5750.
[12] J.T. Kummer, T.W. Dewitt, P.H. Emmett, J. Am. Chem. Soc. 70 (1948) 3632–3643.
[13] D.M. Stockwell, D. Bianchi, C.O. Bennett, J. Catal. 113 (1988) 13–25.
[14] D.J. Dwyer, J.H. Haredenergh, J. Catal. 87 (1984) 66–76.
[15] D.B. Cao, Y.W. Li, J.G. Wang, H.J. Jiao, J. Phys. Chem. C 112 (2008) 14883–14890.
[16] G. Zhao, C. Zhang, S. Qin, H. Xiang, Y. Li, J. Mol. Catal. A 286 (2008) 137–142.
[17] F. Bozso, G. Ertl, M. Grunze, M. Weiss, Appl. Surf. Sci. 1 (1977) 103–119.
[18] E. Chornet, R.W. Couphlin, J. Catal. 27 (1972) 246–265.
[19] Y. Amenomiya, G. Pleizier, J. Catal. 28 (1973) 442–454.
[20] K. Yoshida, G.A. Somorjai, Surf. Sci. 75 (1978) 46–60.
[21] J. Benziger, R.J. Madix, Surf. Sci. 94 (1980) 119–153.
[22] A.M. Baró, W. Erley, Surf. Sci. 112 (1981) L759–L764.
[23] E.A. Kurz, J.B. Hudson, Surf. Sci. 195 (1988) 15–30.
[24] G. Gdowski, R.J. Madix, Surf. Sci. 105 (1981) L307–L311.
[25] C. Brucker, T. Rhodin, J. Catal. 47 (1977) 214–231.
[26] C.-T. Au, C.-F. Ng, M.-S. Liao, J. Catal. 185 (1999) 12–22.
[27] I.M. Ciobîcă, F. Frechard, R.A. van Santen, A.W. Kleyn, J. Hafner, J. Phys. Chem. B 104 (2000) 3364–3369.
[28] B.-T. Teng, W.-X. Huang, F.-M. Wu, Y.-Z. Lan, D.-B. Cao, J. Chem. Phys. 132 (2010), 024715-1-7.
[29] G. Ertl, S.B. Lee, M. Wiess, Surf. Sci. 111 (1981) L711–L715.
[30] J.K. Brown, A.C. Luntz, P.A. Schultz, J. Chem. Phys. 95 (1991) 3767–3774.
[31] D.W. Moon, D.J. Dwyer, S.L. Bernasek, Surf. Sci. 163 (1985) 215–229.
[32] S.D. Cameron, D.J. Dwyer, Surf. Sci. 198 (1988) 315–330.
[33] H. Wan, B. Wu, C. Zhang, H. Xiang, Y. Li, J. Mol. Catal. A 283 (2008) 33–42.
[34] D.-B. Cao, F.-Q. Zhang, Y.-W. Li, H.-J. Jiao, J. Phys. Chem. B 108 (2004) 9094–9104.
[35] M.E. Dry, T. Shingles, L. Boshoff, G.J. Oosthuizen, J. Catal. 15 (1969) 190–199.
[36] F. Bonnet, F. Ropital, P. Lecour, D. Espinat, Y. Huiban, L. Gengembre, Y. Berthier, P. Marcus, Surf. Interface Anal. 34 (2002) 418–422.
[37] M. Textor, I.D. Gay, R. Mason, Proc. R. Soc. Lond. A 356 (1977) 37–45.
[38] K. Kishi, M.W. Roberts, J. Chem. Soc., Faraday Trans. 1 71 (1975) 1715–1720.
[39] H.J. Krebs, H.P. Bonzel, G. Gafner, Surf. Sci. 88 (1979) 269–283.
[40] H.P. Bonzel, H.J. Krebs, Surf. Sci. 91 (1980) 499–513.
[41] A.C. Ferrari, J. Robertson, Phys. Rev. B 61 (2000) 14095–14107.
[42] J. Schwan, S. Ulrich, V. Batori, H. Ehrhardt, S.R.P. Silva, J. Appl. Phys. 80 (1996) 440–447.
[43] S. Urbonaite, L. Hälldahl, G. Svensson, Carbon 46 (2008) 1942–1947.
[44] R.W. Wood, G. Collins, Phys. Rev. 42 (1932) 386–393.
[45] D.E. Jiang, E.A. Carter, Phys. Rev. B 71 (2005), 045402-1-6.
[46] D.-B. Cao, F.-Q. Zhang, Y.-W. Li, J. Wang, H. Jiao, J. Phys. Chem. B 109 (2005) 833–844.
[47] P.E. Nolan, D.C. Lynch, A.H. Cutler, J. Phys. Chem. B 102 (1998) 4165–4175.
[48] W.T. Osterloh, M.E. Cornell, R. Pettit, J. Am. Chem. Soc. 104 (1982) 3759–3761.